PNAS
www.pnas.org

Supplementary Information for

Trait evolution is reversible, repeatable, and decoupled in the soldier caste of turtle ants

Scott Powell[1], Shauna L. Price [1 2], & Daniel J. C. Kronauer[3]

[1] Department of Biological Sciences, George Washington University, Washington DC, USA.

[2] Department of Science and Education, Field Museum of Natural History, Chicago, IL, USA.

[3] Laboratory of Social Evolution and Behavior, The Rockefeller University, New York NY, USA.

Corresponding author: Scott Powell.

Address: George Washington University, Department of Biological Sciences, 800 22nd Street NW, Suite 6000, Science and Engineering Hall, Washington DC 20052, U.S.A.

E-mail: scottpowell@gwu.edu

This PDF file includes:

www.pnas.org/cgi/doi/10.1073/pnas.1913750117

Supplementary Information Text

Soldier morphotype definitions. The soldier morphotype names of square, dome, disc, and dish reflect the key morphological feature of each distinct head type. These are new, taxonomically precise definitions based on differentiated fusion and configuration of the following three homologous structures of the head: 1) the frontal carinae (Fig. S1, blue), 2) the vertexal corners (Fig. S1, pink), and 3) the median-vertexal teeth (Fig. S1, yellow). The vertex (Fig. S1, teal) is also important as a spatial reference point for the relative positioning of the three homologous structures. These morphotype definitions build on previous work that used the disc as a reference phenotype within the group and then identified two additional categories based on the partial presence or complete absence of the disc (1). Our revised morphotypes also correspond to different ecological patterns of nest-entrance selection and associated defensive strategies, each with different mechanical interactions among soldiers and the nest entrance during nest defense (Figs. 1, S2). The four morphotypes are defined as follows:

Square. The frontal carinae (keel-like crest of expanded cuticle) extends posteriorly to form a continuous carinae with the vertexal corners, giving a square shape to the posterior region of the head (Fig. S1, dorsal view). The transition between the head dorsum and the vertex is delimited at the median by distinct median-vertexal teeth. The vertex may slope gently to acutely towards the posterior vertexal margins, but is largely visible in dorsal view and especially towards the vertexal corners.

Dome. The frontal carinae terminate posteriorly before reaching the vertexal corners, and usually over the eyes, while the vertex forms an approximately right-angled delimitation with the head dorsum at the median to create a domed posterior region of the head (Fig. S1, lateral and dorsal view). The domed posterior shape then largely obscures the vertex in dorsal view. The areas between the posterior termination of the frontal carinae and the vertexal corners may be variably rounded to marginate, but not forming carinae. The median-vertexal teeth may be weakly to strongly visible at the right-angled median delimitation between the head dorsum and the vertex, while the transition either side of the median-vertexal teeth may also be variably rounded to marginate, but never forming carinae.

Disc. The frontal carinae form a continuous carinae over the eyes and along the delimitation between the head dorsum and the vertex, ultimately fusing with the median-vertexal teeth posteriorly to create a unified dorsal disc structure (Fig. S1). Distinct median-vertexal teeth may be absent to strongly visible in the posterior margin of the disc. The vertex forms a right-angle to weakly acute angle with the head dorsum at the median (lateral view), while the vertexal corners remain aligned with the posterior margin of the vertex and thus disassociated from the frontal carinae and the overall disc structure.

Dish. The dish morphotype follows the definition of the disc morphotype, but with the frontal carinae and frontal lobes fusing anteriorly to completely cover and overhang the mandibles (Fig. S1, lateral and dorsal views). The posterior margin of the dish may also be further projected posteriorly, creating a strongly acute angle between the head dorsum and the vertex.

Compiling the morphotype dataset. For the present study, focused on maximum functional capabilities of each species and differentiation among species, we standardized

our dataset on the morphotype of the largest soldiers in each species. In a small number of species, the morphotype of the largest soldier specimens can be incompletely formed in the smallest soldier specimens and sometimes more representative of a different morphotype (1, 2). It is also important to note that queens can be placed in the same morphotype as the soldiers in most species (1). Moreover, queens also use their heads for nest-entrance defense before they produce their first soldiers to assume the defensive role. However, the queen head must also accommodate the ocelli (the light sensing organs used in flight) at the rear of the head (light-sensing organs involved in flight; 1). Furthermore, the head phenotype of the queen likely faces different selection pressures and tradeoffs associated with a broader behavioral repertoire that includes dispersal, mating, and colony founding. In contrast, morphotype in the soldier is associated with a more specialized, life-long defensive function and is coupled with caste-specific defensive strategies and behavior (2-5). Accordingly, the defensive morphotype is typically more pronounced in the soldier caste. Our focus here is then on the evolution of soldier morphotype without any direct comparison to similar categorization of queen heads.

Compiling the head width dataset. Our head width dataset was standardized on maximum head width for both soldier and queen castes. We used all available data for caste head widths, with extensive taxonomic data compiled from worldwide museum material (1) serving as the primary source. The collections of SP were then used to update or add data for castes that were poorly represented or unknown in the primary data source. New head width measurements for both soldier and queen castes were taken at the maximum width of the head behind the eyes, matching the procedure used in the primary data source (1). By standardizing on maximum head width, we capture the ecologically meaningful maximum blocking capacity of the soldier caste for each species, as well as the maximum expression of the trait in the queen. This trait value is also robust against two major sources of intraspecific variation in caste size that can occur in ants. First, caste size-distributions typically increase in mean, maximum, and range as ant colonies grow, with the distribution typically stabilizing at reproductive maturity (6). While the source data provide no information about colony growth stage or caste distributional data, precluding summary statistics like mean, the caste maximum is likely to be well-represented across all collections for a species and therefore a robust and comparable trait value across species. Second, ant species are also known to differ in caste size ranges once caste production stabilizes at reproductive maturity (i.e. the distribution of caste size at maturity is a species trait). This is known to be true for a subset of turtle ant species for which complete collections of reproductively mature colonies have been made, and this is associated with the range of entrance sizes that those taxa use (2). By standardizing on maximum head width across species, our analyses can therefore focus on the ecologically meaningful question of maximum blocking capacity across species, without incorporating the more complex and data-intensive question of the range of soldier blocking capacities within a species.

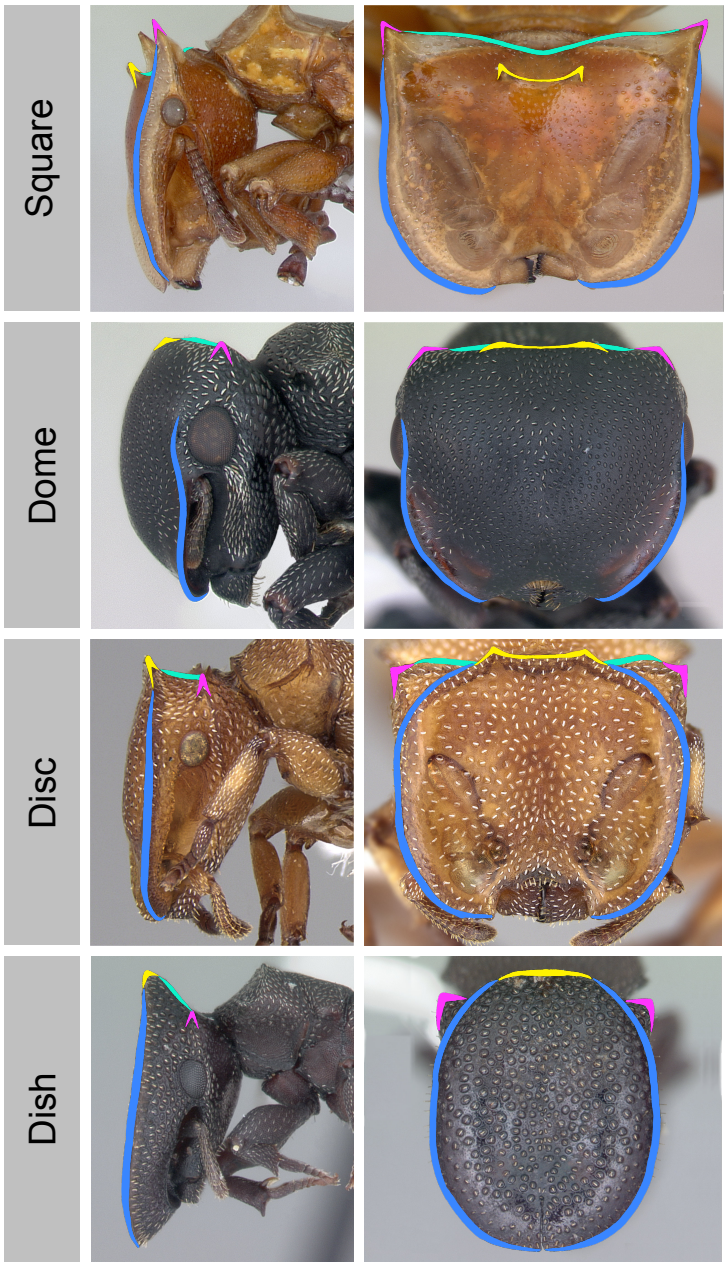

Fig. S1. The four soldier morphotypes present in the turtle ants, defined by the differentiated fusion and configuration of three homologous structures of the head: 1) the frontal carinae (blue), 2) the vertexal corners (pink), and 3) the median-vertexal teeth (yellow). The vertex (teal) is also identified as a spatial reference point for the relative positioning of the homologous structures, with the full surface of the vertex highlighted in lateral view and the posterior vertexal margin highlighted in dorsal view. Pictured representatives are as follows: square morphotype, *Cephalotes clypeatus*; dome morphotype, *Cephalotes pusillus*; disc morphotype, *Cephalotes umbraculatus*; dish morphotype, *Cephalotes varians*. Original specimen images from AntWeb.org.

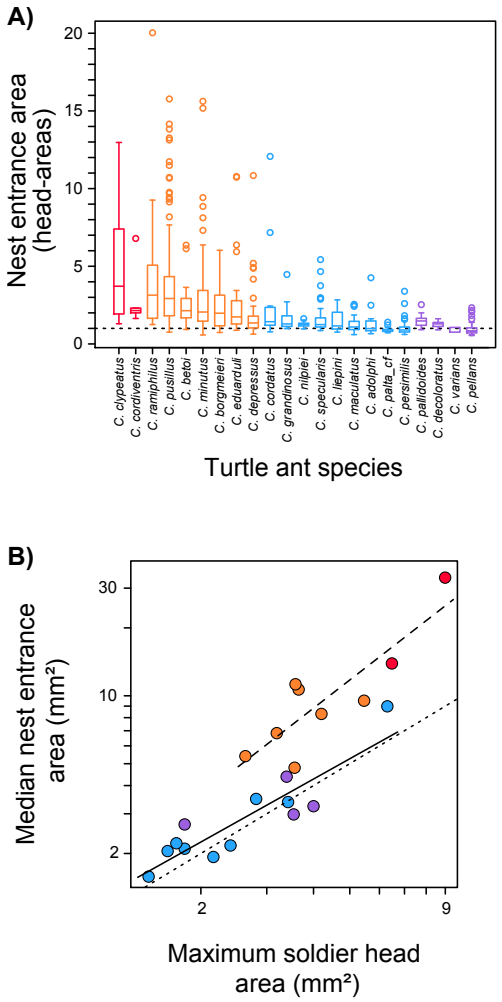

Fig. S2. Relationship between nest entrance usage in nature and the soldier caste for 22 turtle ant species. Representatives of the four soldier morphotypes are identified by the following color coding in both figures: red for square-headed morphotype, orange for dome, blue for disc, and purple for dish. The dataset is an expansion of previously published data for 15 species (2), following the same methods and analyses, but with all species recategorized under the new morphotype definitions used in the present study. **A)** Species distributions for nest-entrance area, represented in soldier head-areas (entrance area divided by maximum soldier head area for each species). The dotted line represents the 1:1 fit between soldier head and entrance hole. In each boxplot, the box encompasses the interquartile range, a line is drawn at the median, the whiskers extend to the upper and lower quartiles, and outliers are shown as open circles. **B)** Relationship between typical (median) nest entrance area and maximum soldier head area for species representing solo-blocking morphotypes (blue and purple points; solid line for linear least-squared regression fit, $F_{1,11}$=43.5, R^2=0.78, P=0.00003) and group-blocking morphotypes (red and orange points; dashed line for linear least-squares regression fit, $F_{1,7}$=20.2, R^2=0.71, P=0.003). There was no significant phylogenetic signal in the residuals for either regression fit (following analyses in (2) and using the phylogenetic tree of Price et a1. (7)). The dotted line represents the 1:1 relationship for a perfect fit between maximum head area of one soldier and median nest entrance area used by the species.

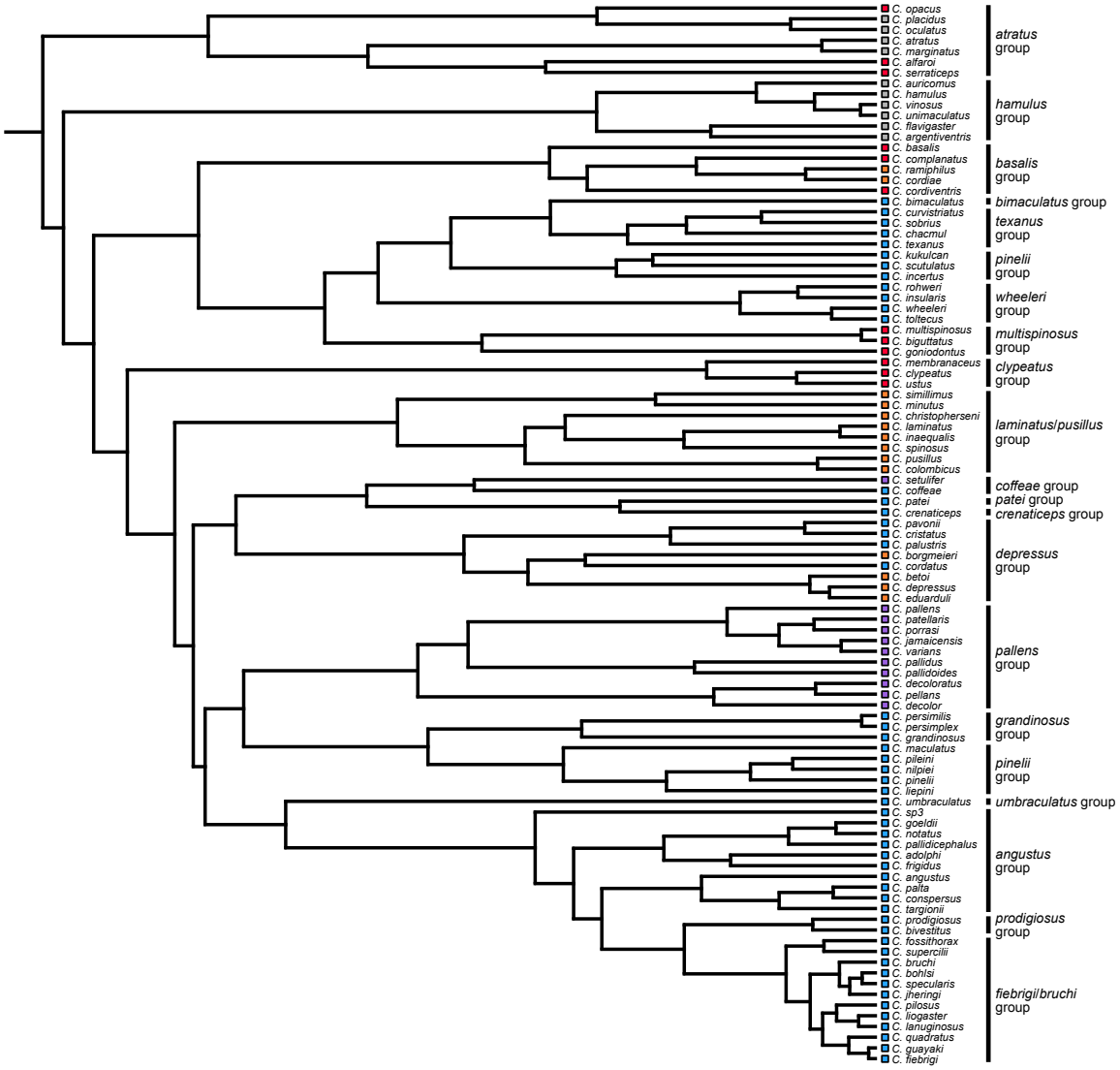

Fig. S3. Phylogeny of the turtle ants (genus *Cephalotes*), showing soldier morphotype (grey for no soldier, red for square-head soldier morphotype, orange for dome, blue for disc, and purple for dish), species names, and species groups. Phylogenetic tree from Price et al. (7), trimmed to include only species for which soldier data are known (including confirmed absence of a soldier caste), with topology matching Fig. 2. The species group names were originally defined by de Andrade & Baroni Urbani (1) as morphological clades. Some of these groups are consolidated (e.g. *laminatus*/*pusillus* groups) or rendered polyphyletic (e.g. *pinelii* group) by more recent molecular and total evidence phylogenies (7, 8), but are shown here for reference.

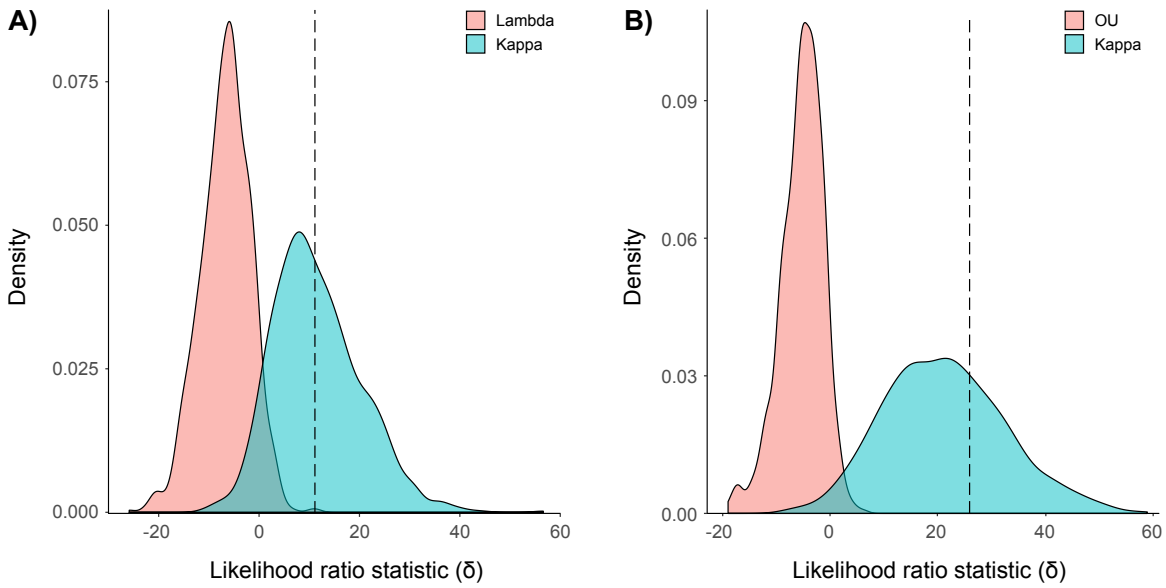

Fig. S4. Example pairwise model comparisons for head width evolution in turtle ant soldiers. Distributions show the likelihood ratio statistic (δ) from the Monte-Carlo method for pairwise model comparisons implemented in the R-package PMC 1.03 (9). A total of 1000 replicates underlie each distribution. **A)** Comparison of the distributions of δ values obtained by bootstrapping under the best-fitting kappa model and the next best-fitting lambda model (pink), as ranked by Akaike Weights. **B)** Comparison of the distribution of δ values obtained by bootstrapping under the best-fitting kappa model and the one-optima OU model (pink). In each pairwise comparison, the dashed vertical line indicates the observed value of δ when the models are fit to the empirical data. In both cases, the limited overlap in distributions and the observed likelihood ratio nearly centered in the kappa distribution indicate that the observed δ value is much more likely under the kappa model. See Table S6 for full set of implemented pairwise model comparisons, P-values, and statistical power.

Table S1. Model fits, estimated root state, and state transitions for soldier morphotype evolution in the turtle ants. Analyses used maximum likelihood estimation, as implemented in the R-packages APE (10). The results are ordered by decreasing Akaike Weights (w), generated using PHYTOOLS (11). A state transition was recognized when the likelihood estimate for one of the five possible states was 75% or more and different from the preceding node. A state transition was also recognized when an extant species had a different state than the preceding ancestral node. The minimum number of state transitions possible for this analysis was four, given the five morphotype states. The total number of state transitions is further broken down into gains (+) and loses (–) for each morphotype. The number of gains for each morphotype is the sum of all the times the state is estimated to have evolved from an ancestor with a different state, plus the root state where appropriate. The number of loses is defined as the number of times a morphotype transitioned to a different state once it has evolved.

Model	AIC	AICΔ	w	Root	Total trans.	Square		Dome		Disc		Dish		No soldier	
						+	–	+	–	+	–	+	–	+	–
Equal rates	105.4028	0.0000	0.9516	Square	11	1	6	4	0	2	5	2	0	3	0
Symm. rates	111.3605	5.9577	0.0484	Square	11	1	6	4	0	2	5	2	0	3	0
All rates diff.	124.8179	19.4151	0.0579e-03	No soldier	12	4	3	4	0	2	4	2	0	1	4

Table S2. Model fits, estimated root state, and total state transitions for soldier morphotype evolution in the turtle ants across a sampling of phylogenetic trees. The maximum clade credibility tree from Price et al. (7) that is used throughout the main analyses is included for contrast. The ten additional trees, sampled from the original phylogenic analyses of Price et al. (7), include the next five trees with the highest clade credibility values, and five trees drawn at random from the posterior distribution of the analysis. See Price et al. (7) for more details on the trees used here. For each tree, the models are ordered by decreasing Akaike Weights (w).

Tree	Model	AIC	AICΔ	w	Root	Total trans.
Max. clade cred.	Equal rates	105.4028	0.0000	0.9516	Square	11
	Symm. rates	111.3605	5.9577	0.0484	Square	11
	All rates diff.	124.8179	19.4151	0.0579e-03	No soldier	12
Clade cred. 2	Equal rates	105.2712	0.0000	0.9618	Square	11
	Symm. rates	111.7242	6.4530	0.0382	Square	11
	All rates diff.	124.6167	19.3455	0.0606e-03	No soldier	14
Clade cred. 3	Equal rates	105.9631	0.0000	0.9560	Square	11
	Symm. rates	112.1223	6.1592	0.0440	Square	11
	All rates diff.	130.7316	24.7685	0.0400e-04	No soldier	18
Clade cred. 4	Equal rates	105.6551	0.0000	0.9615	Square	11
	Symm. rates	112.0951	6.4400	0.0384	Square	11
	All rates diff.	124.5490	18.8939	0.0759e-03	Square	14
Clade cred. 5	Equal rates	105.2343	0.000000	9.617233e-01	Square	11
	Symm. rates	111.6825	6.448126	3.826991e-02	Square	11
	All rates diff.	128.9656	23.731257	6.758855e-06	No soldier	19
Clade cred. 6	Equal rates	105.3685	0.000000	9.614473e-01	Square	11
	Symm. rates	111.8016	6.433068	3.854806e-02	Square	11
	All rates diff.	129.8597	24.491243	4.620827e-06	Square	15
Random 1	Equal rates	108.5671	0.000000	9.344598e-01	Square	11
	Symm. rates	113.8820	5.314927	6.552981e-02	Square	11
	All rates diff.	131.3858	22.818734	1.036419e-05	No soldier	18
Random 2	Equal rates	106.7881	0.000000	9.462766e-01	Square	11
	Symm. rates	112.5256	5.737487	5.372034e-02	Square	11
	All rates diff.	132.0557	25.267587	3.084831e-06	No soldier	18
Random 3	Equal rates	111.2792	0.000000	8.665100e-01	Square	11
	Symm. rates	115.0209	3.741664	1.334387e-01	Square	11
	All rates diff.	130.7483	19.469054	5.130057e-05	No soldier	20
Random 4	Equal rates	106.738	0.000000	9.457760e-01	Square	11
	Symm. rates	112.458	5.720018	5.416294e-02	Square	11
	All rates diff.	126.035	19.297061	6.102175e-05	No soldier	11
Random 5	Equal rates	109.8716	0.000000	0.949452048	Square	11
	Symm. rates	115.7429	5.871393	0.050409951	Square	11
	All rates diff.	127.5443	17.672758	0.000138001	Square	13

Table S3. Table showing estimated morphotype state transitions using Stochastic Character Mapping across three models of state evolution, as implemented in the R-package PHYTOOLS (11). 1000 stochastic character maps were generated and summarized for each model, to provide the estimated root state across replicated mappings and the average number of morphotype transitions. A minimum of four state transitions is possible for this analysis, given the five morphotype states. The total number of state transitions is further broken down into average gains (+) and loses (–) for each morphotype, based on the summary matrix of directional state transitions generated from the PHYTOOLS output.

Model	Root	Avg. trans.	Square		Dome		Disc		Dish		No soldier	
			+	–	+	–	+	–	+	–	+	–
Equal rates	Square	12.4	0.9	6.0	4.0	0.5	2.4	5.2	2.2	0.2	2.9	0.5
Symmetrical	Square	12.7	1.2	6.4	4.0	0.5	2.5	4.8	2.1	0.1	3.0	1.0
All rates different	No soldier	17.6	4.8	2.1	3.6	1.1	8.2	0	1.0	8.6	0	5.8

Table S4. Estimated root state and total state transitions for two simplified binary-state analyses related to morphotype evolution in the turtle ants. The first binary-state analysis addressed the evolution of group-blocking morphotypes versus solo-blocking morphotypes. The second addressed soldier caste presence versus absence. For both analyses, a minimum of one state transition was possible, given the binary-state of the trait being examined. For both analyses, ancestral states were estimated using maximum likelihood estimation under two models of state evolution. A state transition was recognized when likelihood estimates for one of the two possible states was 75% or more and different from the preceding node. State transitions were also recognized when an extant species had a different state than the preceding ancestral node. Analyses were implemented in the R-packages APE (10).

Model	Group-Solo Root	Group-Solo total trans.	Soldier-No soldier Root	Soldier-No soldier total trans.
Equal rates	Group	4	Soldier	3
All Rates Different	Group	4	No soldier	3

Table S5. Fit of models for continuous character evolution to soldier head width data in the turtle ants. Analyses were implemented in R-package PMC 1.03 (9), which calls R-Packages GEIGER (12) OUCH (13) for model fitting and uses a Monte Carlo-based method to generate 95% parameter confidence intervals. The models are ordered by decreasing Akaike weights (w), generated using PHYTOOLS (11).

Model	Model parameters and 95% confidence intervals	AICc	AICcΔ	w
Kappa	kappa=0.060(0.000–0.383); sigsq=0.058(0.029–0.077); z0=2.903(2.397–3.386)	96.82	0.00	9.96e-01
Lambda	lambda=0.819(0.512–0.938); sigsq=0.007(0.004–0.011); z0=2.410(2.031–2.760)	107.95	11.13	3.82e-03
OU2	alpha=2.183 (3.414–53.572); sigsq=1.455 (2.786–45.034); optima1=2.409(1.891–2.643); optima2=1.582(1.878–2.545)	122.02	25.20	3.36e-06
OU	alpha=0.028(0.010–0.062); sigsq=0.025(0.016–0.040); optimum=2.266(1.925–2.571)	122.68	25.86	2.41e-06
Delta	delta=2.585(1.564–3.000); sigsq=0.0090(0.006–0.0130); z0=2.2013(1.937–2.466)	125.63	28.81	5.52e-07
Trend	slope = 2.109(0.003–100.0); sigsq=0.0002(3.220e-06–0.014); z0=2.261(1.937–2.588)	126.27	29.45	4.02e-07
BM	sigsq=0.017 (0.0002–0.0004); z0=2.441(2.354–2.527)	129.98	33.16	6.28e-08
EB	a=-0.000001(-0.027–0.000001); sigsq=0.018(0.013–0.048); z0=2.441(1.793–3.043)	132.12	35.30	2.15e-08
White	sigsq=0.327(0.077–0.140); z0=2.047(1.975–2.120)	157.35	60.53	7.17e-14

Table S6. Significance tests and statistical power for Monte Carlo-based pairwise model comparisons (9). Analyses implemented in the R-package PMC 1.03 (9). For each pairwise model comparison, the observed likelihood ratio statistic (δ) is derived from fitting the models to the original data, the critical null δ provides the critical value for significance testing at 95% confidence intervals, the P-value is testing the hypothesis that the data came from the null versus the test model, and the statistical power of the comparison is also reported.

Model comparison (null vs. test)	Observed δ	Critical null δ	P-value	Power %
Lambda vs. Kappa	11.1272	0.66964	0.001	92.5
OU vs. Kappa	25.8614	0.33078	0.000	98.2
Delta vs. Kappa	28.8127	-0.25050	0.000	99.9
Trend vs. Kappa	29.4445	1.48733	0.000	99.6
BM vs. Kappa	35.3005	2.59697	0.000	100.0
EB vs. Kappa	35.3009	2.42827	0.000	99.9
White vs. Kappa	62.6688	-21.95457	0.000	100.0
OU vs. OU2	3.6229	4.20499	0.070	7.0

Table S7. Model fits across kappa, Brownian motion (BM), single-optimum Ornstein-Uhlenbeck (OU) models, and a set of models that represent Lévy processes with jumps, as implemented in the R-package PULSR (14). The JN model represents a compound Poisson with normally distributed jumps process, while the NIG model represents a normal inverse Gaussian jump process. The BMJH and BMNIG models combined Brownian motion with the Lévy processes implemented in the JN and NIG models, respectively. The models are ordered by decreasing Akaike Weights (w).

Model	Model-specific parameter	AICc	AICcΔ	w
Kappa	kappa=0.0599; sigsq=0.0578; z0=2.9028	96.8198	0.00000	0.49188
JN	tip.sigma= 0.1266; jn.lambda= 0.0374; jn.delta= 0.5039	96.8234	0.0037	0.49097
BMNIG	tip.sigma=0.1242; bm.sigma=0.00001; nig.alpha=1.1964; nig.delta=0.0122	104.4251	7.6054	0.01097
BMJN	tip.sigma=0.1211; bm.sigma=0.0569; jn.lambda=0.0322; jn.delta=0.4259	105.7735	8.9537	0.00559
BM	tip.sigma=0.2492; bm.sigma=0.0782	111.3603	14.5405	0.00034
NIG	tip.sigma=0.2450; nig.alpha=19.4858; nig.delta=0.1211	113.3107	16.4909	0.00013
OU	tip.sigma=0.2491; bm.sigma=0.0784; ou.alpha=0.0001	113.5364	16.7166	0.00012

Table S8. Matrix of morphotype and maximum head width data used in trait evolution analyses. Included taxa are those from the phylogeny of Price et al. (7) with available data for soldier morphotype and head width. Queen head width data is also provided for all species where the queen caste is also known. The matrix was compiled from all available data and images in de Andrade and Baroni Urbani (1), data and specimens from the collections of SP, and from examining type specimen images on AntWeb.org. Soldier morphotype encoding is as follows: 0 for species known to lack a soldier caste, 1 for square-headed soldier morphotype, 2 for dome-headed morphotype, 3 for disc-headed morphotype, and 4 for dish-headed morphotype. Empty blue cells denote species known to lack a soldier caste. Green cells denote no available queen head width data. Red cells denote updated maximum head width data from new specimens in the collection of SP.

Species	Soldier morphotype	Soldier max. head width (mm)	Queen max. head width (mm)
C. adolphi	3	2.00	1.66
C. alfaroi	1	3.60	
C. angustus	3	2.60	2.52
C. argentiventris	0		
C. atratus	0		4.50
C. auricomus	0		2.16
C. basalis	1	3.16	2.96
C. betoi	2	2.26	2.12
C. biguttatus	1	2.06	2.32
C. bimaculatus	3	1.76	1.68
C. bivestitus	3	1.82	1.64
C. bohlsi	3	1.80	
C. borgmeieri	2	2.52	2.16
C. bruchi	3	3.08	2.56
C. chacmul	3	1.04	
C. christopherseni	2	2.60	2.52
C. clypeatus	1	3.84	3.08
C. coffeae	3	1.44	1.44
C. colombicus	2	2.40	2.54
C. complanatus	1	2.96	2.80
C. conspersus	3	1.32	
C. cordatus	3	2.56	1.94
C. cordiae	2	2.12	2.24
C. cordiventris	1	3.08	2.92
C. crenaticeps	3	1.72	1.72
C. cristatus	3	2.40	2.36
C. curvistriatus	3	1.76	1.72
C. decolor	4	2.32	2.00
C. decoloratus	4	2.00	1.60
C. depressus	2	2.22	2.08
C. eduarduli	2	2.56	2.28
C. fiebrigi	3	1.48	1.48
C. flavigaster	0		
C. fossithorax	3	1.80	1.56
C. frigidus	3	1.84	1.60
C. goeldii	3	1.88	1.96
C. goniodontus	1	2.12	
C. grandinosus	3	1.44	1.40

C. guayaki	3	1.16	1.08
C. hamulus	0		2.12
C. inaequalis	2	2.64	3.02
C. incertus	3	1.32	1.22
C. insularis	3	1.84	1.76
C. jamaicensis	4	1.90	
C. jheringi	3	2.00	1.72
C. kukulcan	3	1.44	1.40
C. laminatus	2	2.68	2.76
C. lanuginosus	3	1.96	1.78
C. liepini	3	1.52	
C. liogaster	3	1.92	1.80
C. maculatus	3	1.28	1.22
C. marginatus	0		4.90
C. membranaceus	1	3.00	2.68
C. minutus	2	1.80	1.74
C. multispinosus	1	2.44	2.40
C. nilpiei	3	1.48	
C. notatus	3	1.64	1.64
C. oculatus	0		3.00
C. opacus	1	3.00	3.04
C. pallens	4	2.00	1.60
C. pallidicephalus	3	1.76	1.68
C. pallidoides	4	1.48	1.52
C. pallidus	4	1.64	1.42
C. palta	3	1.76	
C. palustris	3	2.36	
C. patei	3	2.32	2.30
C. patellaris	4	1.88	1.64
C. pavonii	3	2.28	2.08
C. pellans	4	1.78	1.68
C. persimilis	3	1.48	1.64
C. persimplex	3	1.44	1.40
C. pileini	3	1.36	1.28
C. pilosus	3	2.08	1.64
C. pinelii	3	1.44	1.38
C. placidus	0		3.12
C. porrasi	4	1.72	1.56
C. prodigiosus	3	2.76	2.40
C. pusillus	2	2.36	2.36
C. quadratus	3	1.48	
C. ramiphilus	2	2.28	2.00
C. rohweri	3	1.84	1.72
C. scutulatus	3	1.64	1.64
C. serraticeps	1	3.32	3.10
C. setulifer	4	1.36	1.36
C. simillimus	2	1.76	
C. sobrius	3	1.80	1.52
C. sp3	3	1.58	1.40
C. specularis	3	1.88	1.70
C. spinosus	2	2.72	2.84
C. supercilii	3	1.88	1.72

C. targionii	3	1.88	1.64
C. texanus	3	1.56	1.52
C. toltecus	3	1.72	
C. umbraculatus	3	2.56	2.72
C. unimaculatus	0		
C. ustus	1	3.00	
C. varians	4	1.76	1.58
C. vinosus	0		
C. wheeleri	3	1.72	

References

1. de Andrade ML, Baroni Urbani C (1999) Diversity and adaptation in the ant genus *Cephalotes*, past and present. *Stuttgarter Beitr Naturk Ser B* 271:1–889.

2. Powell S (2016) A comparative perspective on the ecology of morphological diversification in complex societies: nesting ecology and soldier evolution in the turtle ants. *Behav Ecol Sociobiol* 70(7):1075–1085.

3. Powell S (2008) Ecological specialization and the evolution of a specialized caste in *Cephalotes* ants. *Func Ecol* 22(5):902–911.

4. Powell S, Dornhaus A (2013) Soldier-based defences dynamically track resource availability and quality in ants. *Anim Behav* 85(1):157–164.

5. Powell S, Donaldson-Matasci M, Woodrow-Tomizuka A, Dornhaus A (2017) Context-dependent defences in turtle ants: Resource defensibility and threat level induce dynamic shifts in soldier deployment. *Func Ecol* 31(12):2287–2298.

6. Hölldobler B, Wilson EO (1990) *The ants* (Harvard University Press, Cambridge, Mass.).

7. Price SL, Etienne RS, Powell S (2016) Tightly congruent bursts of lineage and phenotypic diversification identified in a continental ant radiation. *Evolution* 70(4):903–912.

8. Price SL, et al. (2014) Renewed diversification is associated with new ecological opportunity in the Neotropical turtle ants. *J Evol Biol* 27(2):242–258.

9. Boettiger C, Coop G, Ralph P (2012) Is your phylogeny informative? Measuring the power of comparative methods. *Evolution* 66(7):2240–2251.

10. Paradis E, Claude J, Strimmer K (2004) APE: Analyses of Phylogenetics and Evolution in R language. *Bioinformatics* 20(2):289–290.

11. Revell LJ (2012) phytools: an R package for phylogenetic comparative biology (and other things). *Methods Ecol Evol* 3(2):217–223.

12. Pennell MW, et al. (2014) geiger v2.0: an expanded suite of methods for fitting macroevolutionary models to phylogenetic trees. *Bioinformatics* 30(15):2216–2218.

13. King AA, Butler MA (2009) *ouch: Ornstein-Uhlenbeck models for phylogenetic comparative hypotheses (R package)* Available at: https://kingaa.github.io/ouch/.

14. Landis MJ, Schraiber JG (2017) Pulsed evolution shaped modern vertebrate body sizes. *PNAS* 114(50):13224–13229.